Title
High-Photovoltage Silicon Nanowire for Biological Cofactor Production

Journal
Journal of the American Chemical Society, 145(36)

ISSN
0002-7863

Authors
Lineberry, Elizabeth
Kim, Jinhyun
Kim, Jimin
et al.

Publication Date
2023-09-13

DOI
10.1021/jacs.3c06243

Peer reviewed

High-Photovoltage Silicon Nanowire for Biological Cofactor Production

Elizabeth Lineberry[1,†], Jinhyun Kim[2,†], Jimin Kim[3], Inwhan Roh[1], Jia-An Lin[1], and Peidong Yang[1,3,4,5,6,*]

[1]Department of Chemistry, University of California, Berkeley, Berkeley, CA 94720, USA
[2]Department of Chemical and Biomolecular Engineering, University of California, Berkeley, Berkeley, CA 94720, USA
[3]Department of Materials Science and Engineering, University of California, Berkeley, Berkeley, CA 94720, USA
[4]Chemical Sciences Division, Lawrence Berkeley National Laboratory, Berkeley, CA 94720, USA
[5]Materials Sciences Division, Lawrence Berkeley National Laboratory, Berkeley, CA 94720, USA
[6]Kavli Energy Nanosciences Institute, Berkeley, CA 94720, USA
[†]These authors contributed equally to this work.
[*]Correspondence: p_yang@berkeley.edu

KEYWORDS: Silicon nanowire, photovoltage, photoelectrochemistry, biological cofactor, redox mediator

ABSTRACT: Photocathodic conversion of NAD^+ to NADH cofactor is a promising platform for activating redox biological catalysts and enzymatic synthesis using renewable solar energy. However, many photocathodes suffer from a low photovoltage, consequently requiring a high cathodic bias for NADH production. Here, we report an n^+p-type silicon nanowire (n^+p-SiNW) photocathode having a photovoltage of 435 mV to drive energy-efficient NADH production. The enhanced band bending at the n^+/p interface accounts for the high photovoltage, which conduces to a benchmark onset potential [0.393 V vs. the reversible hydrogen electrode (V_{RHE})] for SiNW-based photocathodic NADH generation. In addition, the n^+p-SiNW nanomaterial exhibits a Faradaic efficiency of 84.7% and a conversion rate of 1.63 μmol h^{-1} cm^{-1} at 0.2 V_{RHE}, which is the lowest cathodic potential to achieve the maximum productivity among SiNW-sensitized cofactor production.

In CO_2-reductive photosynthetic biohybrid systems, biogenic redox molecules (e.g., nicotinamide-based cofactors, ferredoxin) function as redox communicators between solar-harvesting nanomaterials and bacterial oxidoreductases.[1-5] Photocatalytic nanomaterials [e.g., CdS, gold nanocluster, silicon nanowire (SiNW)] efficiently and steadily convert light energy into photoexcited electrons and/or H_2.[6-7] These reducing equivalents are transferred into acetogenic bacteria (e.g., *Moorella thermoacetica*, *Sporomusa ovata*) and used to regenerate biological electron shuttles, which trigger highly selective multienzymatic CO_2 fixation in the Wood-Ljungdahl pathway (WLP).[6] However, the underlying pathway for electron transfer from light-active nanomaterials to whole-cell biocatalytic machineries remains largely ambiguous because of complicated features of the biotic/abiotic interfaces.[8]

This fundamental question at the molecular level can be addressed by constructing photoelectrochemical (PEC) regeneration of 1,4-dihydronicotinamide adenine dinucleotide (NADH) or its phosphorylated form (NADPH) from NAD^+ or $NADP^+$, respectively. This is because (i) NAD(P)H is the key redox cofactor that provides its electrons for over 80% of redox enzymes (e.g., dehydrogenases and reductases in the WLP),[6, 9-15] and (ii) PEC platform offers a facile method for analyzing redox phenomena associated with biological catalysts.[16-21]

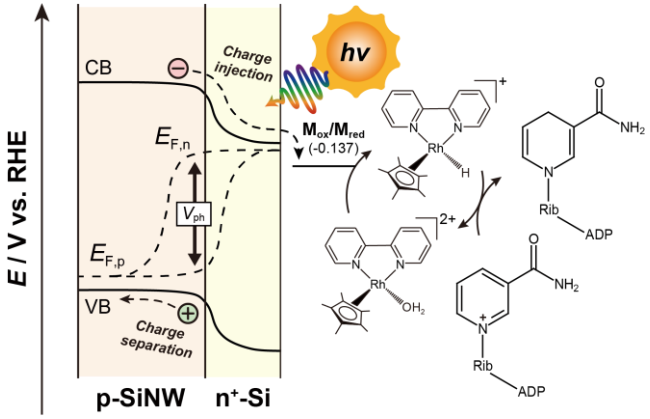

Scheme 1. Illustration of photocathodic NADH production driven by n^+p-SiNW. The photocathode absorbs solar light to generate photoexcited charge carriers and a corresponding photovoltage. The photoexcited electrons are transferred to $\mathbf{M_{ox}}$ because the quasi-Fermi level of the electrons is more negative than the redox potential of $\mathbf{M_{ox}/M_{red}}$. The $\mathbf{M_{red}}$ regiospecifically transfers its hydride ion to the C4 atom of the NAD^+, which results in the formation of enzymatically active NADH. V_{ph}: photovoltage. CB: conduction band. VB: valence band. $E_{F,n}$: quasi-Fermi level of electrons. $E_{F,h}$: quasi-Fermi level of holes. Rib: ribose. ADP: adenosine diphosphate. $\mathbf{M_{ox}}$: $[Cp^*Rh(bpy)H_2O]^{2+}$. $\mathbf{M_{red}}$: $[Cp^*Rh(bpy)H]^+$.

For photocathodic NADH regeneration, p-type SiNW (p-SiNW) is a promising energy nanomaterial because of its many PEC advantages[22-24] such as (i) enhanced photon harvesting through light trapping properties, (ii) better charge separation efficiency due to shorter migration length of photoexcited electrons, (iii) broad solar absorption caused by low bandgap (~1.1 eV), and (iv) increased reaction turnover because of large catalytic surface area. Several p-SiNW-based photocathodes (e.g., hydrogen-terminated p-SiNW,[25] hydrogen-terminated p-SiNW with platinum nanoparticles,[26] p-SiNW[27]) have been reported to regiospecifically produce NADH through the conversion of $[Cp^*Rh(bpy)H_2O]^{2+}$ (**M_{ox}**; $Cp^* = C_5Me_5$, bpy = 2,2'-bipyridine) to $[Cp^*Rh(bpy)H]^+$ (**M_{red}**). These precedent works have focused on interface chemistry of p-Si electrodes for better charge transfer to **M_{ox}**. However, band structure engineering of Si photocathodes has not been studied for obtaining insights into low-bias NADH formation.

In this study, we enhanced the photovoltage (V_{ph}) of p-SiNW photocathode by constructing a buried n^+p radial junction for energy-efficient NADH production under solar light. As illustrated in **Scheme 1**, we introduced a n^+ layer into p-SiNW arrays, which increases the band bending at the n^+/p interface and consequently enhances the p-SiNW's V_{ph} (435 mV). The energy nanomaterial transfers its photoexcited electrons to **M_{ox}** mediator with a benchmark onset potential (E_{onset}) of 0.393 V versus the reversible hydrogen electrode (V_{RHE}) among reported SiNW-based photocathodes[25-27]. As a result, the n^+p-SiNW photocathode achieves **M_{red}**-mediated conversion of NAD^+ to NADH, yielding a Faradaic efficiency (FE) of 84.7% and conversion rate of 1.63 μmol h^{-1} cm^{-1} at 0.2 V_{RHE}. In addition, the stable photocathodic system maintains NADH formation for at least 12 h at the low cathodic potential.

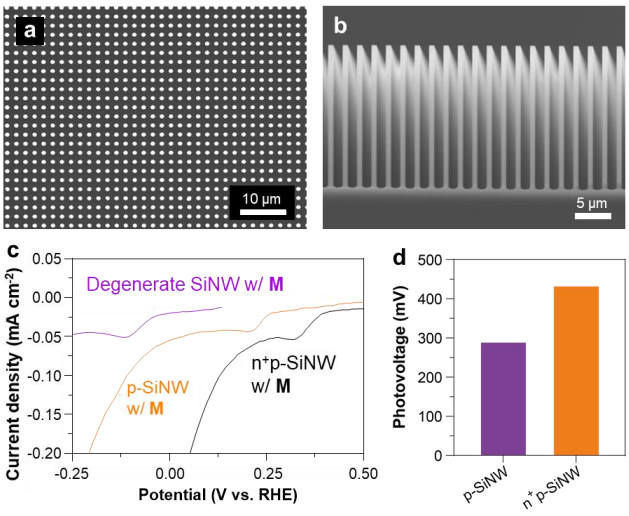

Figure 1. Photocathodic reduction of $[Cp^*Rh(bpy)H_2O]^{2+}$ driven by SiNW-based catalysts. (**a**) Plan-view and (**b**) cross-sectional tilted scanning electron microscopic (SEM) image of p-SiNW electrode. (**c**) Linear sweep voltammograms of degenerate SiNW, p-SiNW, and n^+p-SiNW for **M_{ox}** reduction under 1-sun illumination. Electrolyte solution: O_2-depleted phosphate buffer (100 mM, pH 7.2). Scan rate: 10 mV s^{-1}. (**d**) Comparison of photovoltages between p-SiNW and n^+p-SiNW.

We fabricated a p-type boron-doped SiNW (**Figures 1a and 1b**) through deep reactive ion etching of patterned single-crystalline Si wafers according to the reported method[22, 28]. We investigated **M_{ox}**'s reduction behaviors on the as-synthesized p-SiNW in a two-compartment, three-electrode configuration under 1-sun illumination (air mass 1.5 global, 100 mW cm^{-2}). In this experiment, we used degenerate SiNW to estimate the V_{ph} of the p-SiNW because the degenerate SiNW exhibits a metallic conductivity under dark conditions (**Figure S1**) and can serve as the baseline for estimating semiconducting SiNW's V_{ph}. According to the linear sweep voltammetric analysis (**Figures 1c and S2**), the p-SiNW exhibited the E_{onset} for reduction of **M_{ox}** to **M_{red}** at 0.250 V_{RHE} with a V_{ph} of 292 mV in an O_2-depleted phosphate buffer (100 mM, pH 7.2). In addition, we observed the p-SiNW's peak current at around 0.212 V_{RHE} (**Figure 1c**), which is consistent with early reports[16-17, 26, 29-30] in (photo)cathodic conversion of **M_{ox}** to **M_{red}**; the peak current originates from a slower migration of **M_{ox}** from the bulk of the electrolyte to the catalyst's surface than **M_{ox}**'s reduction kinetics.

Shifting E_{onset} more anodically can achieve energy-efficient photocathodic production of NADH. Thus, we constructed a radial n^+p junction on the p-SiNW arrays by introducing arsenic atoms on the surface of the p-SiNW according to the literature[22, 31-32]. The buried n^+p interface induces a built-in electric field that enhances the separation of photoinduced charge carriers inside the photocathode.[33-35] The strategy boosts V_{ph} by increasing the band bending at the buried n^+p junction relative to the p-SiNW|electrolyte interface.[35] Note that p-SiNW and n^+p-SiNW exhibit the almost identical length and diameter (**Figure S3**). We found that the doping shifted the E_{onset} of **M_{ox}** reduction more positively by 143 mV (**Figure 1c**), which we ascribe to the increased V_{ph} (435 mV) of n^+p-SiNW (**Figure 1d**). The E_{onset} is higher than those of other SiNW-based photocathodes[25-27] for **M_{ox}** reduction (**Table S1**).

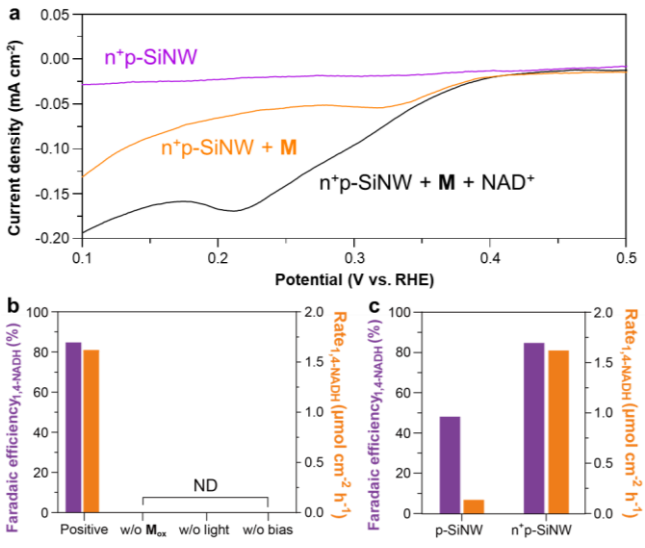

Figure 2. n^+p-SiNW-sensitized conversion of NAD^+ to NADH. (**a**) Changes in photocathodic currents of n^+p-SiNW with the sequential addition of **M_{ox}** and NAD^+. Scan rate: 10 mV s^{-1}. (**b**) Control experiments for photocathodic NADH formation driven by n^+p-SiNW. (**c**) Comparison of Faradaic efficiency and

production rate between p-SiNW and n⁺p-SiNW at 0.2 V_{RHE}. Electrolyte in (**a-c**): 0.25 mM $\mathbf{M_{ox}}$ and 1 mM NAD^+ in an O_2-depleted phosphate buffer (27 mL, 100 mM, pH 7.2). Light intensity in (**a-c**): 1 sun (air mass 1.5 global, 100 mW cm^{-2}).

We further demonstrated the transfer of photoexcited electrons from n⁺p-SiNW to NAD^+ via $\mathbf{M_{red}}$ redox catalyst. Linear sweep voltammograms show that the addition of 1 mM NAD^+ increased the cathodic current relating to $\mathbf{M_{ox}}$'s reduction under 1-sun irradiation (**Figure 2a**). We attribute it to the catalytic effect of $\mathbf{M_{red}}$ in electron transfer to NAD^+. In contrast, the n⁺p-SiNW exhibited a negligible change in the photocathodic current when the catholyte contained NAD^+ only (**Figure S4**). This result indicates no direct delivery of photoexcited electrons to NAD^+ and importance[10-11] of $\mathbf{M_{ox}}$ in producing NADH under milder cathodic potentials.

Having substantiated the charge transfer from n⁺p-SiNW to NAD^+, we advanced to photocathodic conversion of NAD^+ to NADH. We conducted controlled potential photoelectrolysis (1 sun, 0.2 V_{RHE}) and quantified NADH using quantitative ^1H nuclear magnetic resonance (NMR) spectroscopy. This is because the traditional ultraviolet-visible spectroscopic tool does not effectively differentiate between 1,4-NADH (340 nm), 1,6-NADH (345 nm), and NAD dimers (around 340 nm).[36] We observed 1,4-NADH's characteristic peak[13, 16] at ~6.96 ppm in ^1H NMR spectrum after the photoelectrocatalysis (**Figure S5**). We confirmed the n⁺p-SiNW-driven formation of only 1,4-NADH using malate dehydrogenase-based enzymatic assay (**Figure S6**). The n⁺p-SiNW produced NADH with a FE of 84.7% and a conversion rate of 1.63 μmol h^{-1} cm^{-1} in an O_2-depleted phosphate buffer (27 mL, 100 mM, pH 7.2), and the photocathodic reaction required $\mathbf{M_{ox}}$, light, and electrical bias (**Figure 2b**). The FE and conversion rate of the n⁺p-SiNW were around 1.86 and 12.1 times higher, respectively, than those of p-SiNW at 0.2 V_{RHE} (**Figure 2c**), highlighting the importance of a high V_{ph} in efficient NADH production at a mild cathodic potential. When we applied stronger cathodic potentials, n⁺p-SiNW and p-SiNW exhibited similar FEs, which further demonstrates the impact of V_{ph} on efficiencies at milder potentials (**Figure S7**).

We investigated the effect of the applied potential on the FEs and PEC conversion rates. The FE and rate reached a maximum at 0.2 V_{RHE} (**Figure 3**). The applied potential is milder (i.e., more positive) than those (e.g., -0.1485 V_{RHE}, -0.05 V_{RHE}) used to obtain the maximum production rate in reported SiNW-based photocathodes[26-27]; we ascribe it to the high V_{ph} of the n⁺p-SiNW photocathode. The FEs decreased with increasing cathodic potentials higher than 0.2 V_{RHE}, which we attribute the hydrogen evolution reaction driven by $\mathbf{M_{red}}$ and n⁺p-SiNW (**Figure 3**). According to the literature,[27, 37-38] $\mathbf{M_{red}}$ and n⁺p-SiNW perform H_2 production under aqueous environments, and the kinetics of n⁺p-SiNW's H_2 evolution become faster as the applied potential decreases. Albeit the FE drop, the conversion rates for NADH formation remained almost constant at approximately 1.0 μmol h^{-1} cm^{-1} even at more negative potentials. It suggests the constant flow of photoexcited electrons from n⁺p-SiNW to $\mathbf{M_{ox}}$ against competing HER.

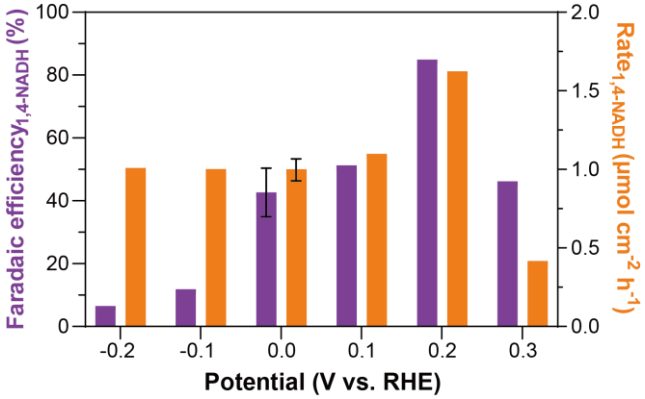

Figure 3. Influence of potential on solar-driven production of NADH. Catholyte: 0.25 mM $\mathbf{M_{ox}}$ and 1 mM NAD^+ in a N_2-enriched phosphate buffer (27 mL, 100 mM, pH 7.2). Light source: xenon lamp (1 sun). Photocathode: n⁺p-SiNW. The enzymatic active NADH (i.e., 1,4-NADH) was quantified using quantitative ^1H nuclear magnetic resonance spectroscopy. Error bar: standard deviation (n = 3).

Next, we investigated the stability of the n⁺p-SiNW photocathode at 0.2 V_{RHE} and 1 sun in a N_2-enriched phosphate buffer (27 mL, 100 mM, pH 7.2). As displayed in **Figures 4a and S8**, we observed a gradual conversion of NAD^+ to NADH for 12 h, which is longer than those (e.g., equal or less than 6 h) of reported SiNW-based photocathodes[25-26]. In addition, we found a negligible change in n⁺p-SiNW's morphology after the photocathodic reaction (**Figures 4b, 4c, and S9**). It indicates the robustness of the nanomaterial, which is a desirable property because of instability issue[39-40] of many photocathodes. Follow-up studies should aim to accelerate the photocathodic NADH generation through, for example, (i) adjustment of band alignment[41] to augment V_{ph}, (ii) functionalization of SiNW arrays with $\mathbf{M_{ox}}$ to boost charge transfer, and (iii) modification of $\mathbf{M_{ox}}$'s molecular structure to tune its redox potential. In addition, the suppression of the n⁺p-SiNW-driven H_2 evolution would enhance the FE for NADH production. These attempts will lay the foundation for energy-efficient electron transfer to biological catalysts[8, 42-43] (e.g., acetogens, redox enzymes) for photobiosynthesis of valuable compounds.

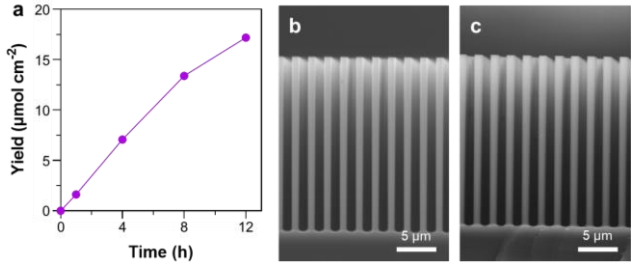

Figure 4. Long-term controlled potential photoelectrolysis for NADH regeneration. (**a**) Time profile of NADH formation driven by n⁺p-SiNW photocathode. Catholyte: 0.25 mM $\mathbf{M_{ox}}$ and 1 mM NAD^+ in an O_2-depleted phosphate buffer (27 mL, 100 mM, pH 7.2). Light intensity: 1 sun. Applied potential: 0.2 V_{RHE}. Cross-sectional SEM images of n⁺p-SiNW (**b**) before and (**c**) after photoelectrocatalysis.

In conclusion, this study reveals the importance of V_{ph} in low-bias production of NADH under solar light. The

construction of a buried n^+p junction on the p-SiNW surface gave rise to an increased V_{ph} (from 292 to 435 mV), a benchmark E_{onset} for $\mathbf{M_{ox}}$ reduction (0.393 V_{RHE}), and an accelerated charge separation through the bulk SiNW, due to the built-in electric field. This improvement led n^+p-SiNW photocathode to achieve the rate of NADH formation (1.63 μmol h^{-1} cm^{-1}) and FE (84.7%) that are 12.1 and 1.86 times higher, respectively, than those of p-SiNW at 0.2 V_{RHE}. Furthermore, the n^+p-SiNW's robustness enabled the steady NADH generation for at least 12 h. The SiNW array having a high V_{ph} continues to be a model platform for energy-efficient production of biological redox cofactors to optimize the performance of photosynthetic biohybrid systems.

ASSOCIATED CONTENT

Supporting Information. The material is available free of charge via the Internet at http://pubs.acs.org. Experimental methods, comparison of $\mathbf{M_{ox}}$ reduction between reported photocathodes, photocathodic activities of SiNW-based electrodes, SEM image of n^+p-SiNW, ^1H NMR analysis, and enzymatic assay.

AUTHOR INFORMATION

Corresponding Author

*Peidong Yang; Email: p_yang@berkeley.edu

Author Contributions

†E.L. and J.K. contributed equally to this work.

Funding Sources

This work was supported by the NSF under grant DMR-2217161.

Notes

The authors declare no competing financial interest.

ACKNOWLEDGMENT

We thank the nanofabrication facilities and entire staff of the Marvell Nanofabrication Laboratory. We thank Dr. Hasan Celik and UC Berkeley's NMR facility in the College of Chemistry (CoC-NMR) for spectroscopic assistance. Instruments in the CoC-NMR are supported in part by NIH S10OD024998. We appreciate Yu Shan from Peidong Yang's group (University of California, Berkeley) for high-magnification scanning electron microscopic images. E.L. gratefully acknowledges support from the National Defense Science and Engineering Graduate (NDSEG) Fellowship.

REFERENCES

1. Cestellos-Blanco, S.; Zhang, H.; Kim, J. M.; Shen, Y.-x.; Yang, P., Photosynthetic semiconductor biohybrids for solar-driven biocatalysis. *Nat. Catal.* **2020,** *3* (3), 245-255.
2. Liu, C.; Gallagher, J. J.; Sakimoto, K. K.; Nichols, E. M.; Chang, C. J.; Chang, M. C. Y.; Yang, P., Nanowire–Bacteria Hybrids for Unassisted Solar Carbon Dioxide Fixation to Value-Added Chemicals. *Nano Lett.* **2015,** *15* (5), 3634-3639.
3. Sakimoto, K. K.; Wong, A. B.; Yang, P., Self-photosensitization of nonphotosynthetic bacteria for solar-to-chemical production. *Science* **2016,** *351* (6268), 74-77.
4. Sakimoto, K. K.; Kornienko, N.; Yang, P., Cyborgian Material Design for Solar Fuel Production: The Emerging Photosynthetic Biohybrid Systems. *Acc. Chem. Res.* **2017,** *50* (3), 476-481.
5. Zhang, H.; Liu, H.; Tian, Z.; Lu, D.; Yu, Y.; Cestellos-Blanco, S.; Sakimoto, K. K.; Yang, P., Bacteria photosensitized by intracellular gold nanoclusters for solar fuel production. *Nat. Nanotechnol.* **2018,** *13* (10), 900-905.
6. Yang, P.; Cai, R.; Kim, J. M.; Cestellos-Blanco, S.; Jin, J., Microbes 2.0: Engineering Microbes with Nanomaterials. *ACM* **2020,** *1* (1), 36-41.
7. Kim, J.; Park, C. B., Artificial photosynthetic biohybrids for CO_2 and N_2 fixation. *Chem Catal.* **2022,** *2* (10), 2425-2427.
8. Yang, P., Liquid Sunlight: The Evolution of Photosynthetic Biohybrids. *Nano Lett.* **2021,** *21* (13), 5453-5456.
9. Kornienko, N.; Zhang, J. Z.; Sakimoto, K. K.; Yang, P.; Reisner, E., Interfacing nature's catalytic machinery with synthetic materials for semi-artificial photosynthesis. *Nat. Nanotechnol.* **2018,** *13* (10), 890-899.
10. Kim, J.; Park, C. B., Collaborative catalysis for solar biosynthesis. *Trends Chem.* **2023,** *5* (2), 133-146.
11. Kim, J.; Park, C. B., Shedding light on biocatalysis: photoelectrochemical platforms for solar-driven biotransformation. *Curr. Opin. Chem. Biol.* **2019,** *49*, 122-129.
12. Kim, J.; Lee, S. H.; Tieves, F.; Choi, D. S.; Hollmann, F.; Paul, C. E.; Park, C. B., Biocatalytic C=C Bond Reduction through Carbon Nanodot-Sensitized Regeneration of NADH Analogues. *Angew. Chem. Int. Ed.* **2018,** *57* (42), 13825-13828.
13. Kim, J.; Lee, S. H.; Tieves, F.; Paul, C. E.; Hollmann, F.; Park, C. B., Nicotinamide adenine dinucleotide as a photocatalyst. *Sci. Adv.* **2019,** *5* (7), eaax0501.
14. Le, T.-K.; Kim, J.; Anh Nguyen, N.; Huong Ha Nguyen, T.; Sun, E.-G.; Yee, S.-M.; Kang, H.-S.; Yeom, S.-J.; Beum Park, C.; Yun, C.-H., Solar-Powered Whole-Cell P450 Catalytic Platform for C-Hydroxylation Reactions. *ChemSusChem* **2021,** *14* (15), 3054-3058.
15. Kim, J.; Nguyen, T. V. T.; Kim, Y. H.; Hollmann, F.; Park, C. B., Lignin as a multifunctional photocatalyst for solar-powered biocatalytic oxyfunctionalization of C–H bonds. *Nat. Synth.* **2022,** *1* (3), 217-226.
16. Kim, J.; Jang, J.; Hilberath, T.; Hollmann, F.; Park, C. B., Photoelectrocatalytic biosynthesis fuelled by microplastics. *Nat. Synth.* **2022,** *1* (10), 776-786.
17. Kim, J.; Lee, Y. W.; Choi, E.-G.; Boonmongkolras, P.; Jeon, B. W.; Lee, H.; Kim, S. T.; Kuk, S. K.; Kim, Y. H.; Shin, B.; Park, C. B., Robust FeOOH/$BiVO_4$/Cu(In, Ga)Se_2 tandem structure for solar-powered biocatalytic CO_2 reduction. *J. Mater. Chem. A* **2020,** *8* (17), 8496-8502.
18. Kim, J.; Um, Y.; Han, S.; Hilberath, T.; Kim, Y. H.; Hollmann, F.; Park, C. B., Unbiased Photoelectrode Interfaces for Solar Coupling of Lignin Oxidation with

Biocatalytic C═C Bond Hydrogenation. *ACS Appl. Mater. Interfaces* **2022,** *14* (9), 11465-11473.
19. Kim, C. H.; Kim, J.; Hollmann, F.; Park, C. B., Photoelectrocatalytic N_2 fixation and C-H oxyfunctionalization driven by H_2O oxidation. *Appl. Catal. B Environ.* **2023,** *336*, 122925.
20. Lee, C. H.; Kim, J.; Park, C. B., Z-Schematic Artificial Leaf Structure for Biosolar Oxyfunctionalization of Hydrocarbons. *ACS Energy Lett.* **2023,** *8* (6), 2513-2521.
21. Choi, D. S.; Kim, J.; Hollmann, F.; Park, C. B., Solar-Assisted eBiorefinery: Photoelectrochemical Pairing of Oxyfunctionalization and Hydrogenation Reactions. *Angew. Chem. Int. Ed.* **2020,** *59* (37), 15886-15890.
22. Roh, I.; Yu, S.; Lin, C.-K.; Louisia, S.; Cestellos-Blanco, S.; Yang, P., Photoelectrochemical CO_2 Reduction toward Multicarbon Products with Silicon Nanowire Photocathodes Interfaced with Copper Nanoparticles. *J. Am. Chem. Soc.* **2022,** *144* (18), 8002-8006.
23. Deng, J.; Su, Y.; Liu, D.; Yang, P.; Liu, B.; Liu, C., Nanowire Photoelectrochemistry. *Chem. Rev.* **2019,** *119* (15), 9221-9259.
24. Jiang, C.; Moniz, S. J. A.; Wang, A.; Zhang, T.; Tang, J., Photoelectrochemical devices for solar water splitting – materials and challenges. *Chem. Soc. Rev.* **2017,** *46* (15), 4645-4660.
25. Son, E. J.; Ko, J. W.; Kuk, S. K.; Choe, H.; Lee, S.; Kim, J. H.; Nam, D. H.; Ryu, G. M.; Kim, Y. H.; Park, C. B., Sunlight-assisted, biocatalytic formate synthesis from CO_2 and water using silicon-based photoelectrochemical cells. *Chem. Commun.* **2016,** *52* (62), 9723-9726.
26. Lee, S. H.; Ryu, G. M.; Nam, D. H.; Kim, J. H.; Park, C. B., Silicon Nanowire Photocathodes for Light-Driven Electroenzymatic Synthesis. *ChemSusChem* **2014,** *7* (11), 3007-3011.
27. Zhang, B.; Xu, S.; He, D.; Chen, R.; He, Y.; Fa, W.; Li, G.; Wang, D., Photoelectrochemical NADH regeneration is highly sensitive to the nature of electrode surface. *J. Chem. Phys.* **2020,** *153* (6), 064703.
28. Kim, J.; Cestellos-Blanco, S.; Shen, Y.-x.; Cai, R.; Yang, P., Enhancing Biohybrid CO_2 to Multicarbon Reduction via Adapted Whole-Cell Catalysts. *Nano Lett.* **2022,** *22* (13), 5503-5509.
29. Lee, Y. W.; Boonmongkolras, P.; Son, E. J.; Kim, J.; Lee, S. H.; Kuk, S. K.; Ko, J. W.; Shin, B.; Park, C. B., Unbiased biocatalytic solar-to-chemical conversion by FeOOH/$BiVO_4$/perovskite tandem structure. *Nat. Commun.* **2018,** *9* (1), 4208.
30. Kuk, S. K.; Singh, R. K.; Nam, D. H.; Singh, R.; Lee, J.-K.; Park, C. B., Photoelectrochemical Reduction of Carbon Dioxide to Methanol through a Highly Efficient Enzyme Cascade. *Angew. Chem. Int. Ed.* **2017,** *56* (14), 3827-3832.
31. Su, Y.; Liu, C.; Brittman, S.; Tang, J.; Fu, A.; Kornienko, N.; Kong, Q.; Yang, P., Single-nanowire photoelectrochemistry. *Nat. Nanotechnol.* **2016,** *11* (7), 609-612.
32. Lin, J.-A.; Roh, I.; Yang, P., Photochemical Diodes for Simultaneous Bias-Free Glycerol Valorization and Hydrogen Evolution. *J. Am. Chem. Soc.* **2023,** *145* (24), 12987-12991.
33. Christesen, J. D.; Zhang, X.; Pinion, C. W.; Celano, T. A.; Flynn, C. J.; Cahoon, J. F., Design Principles for Photovoltaic Devices Based on Si Nanowires with Axial or Radial p–n Junctions. *Nano Lett.* **2012,** *12* (11), 6024-6029.
34. Boettcher, S. W.; Warren, E. L.; Putnam, M. C.; Santori, E. A.; Turner-Evans, D.; Kelzenberg, M. D.; Walter, M. G.; McKone, J. R.; Brunschwig, B. S.; Atwater, H. A.; Lewis, N. S., Photoelectrochemical Hydrogen Evolution Using Si Microwire Arrays. *J. Am. Chem. Soc.* **2011,** *133* (5), 1216-1219.
35. Andrei, V.; Roh, I.; Yang, P., Nanowire photochemical diodes for artificial photosynthesis. *Sci. Adv.* **2023,** *9* (6), eade9044.
36. Saba, T.; Li, J.; Burnett, J. W. H.; Howe, R. F.; Kechagiopoulos, P. N.; Wang, X., NADH Regeneration: A Case Study of Pt-Catalyzed NAD^+ Reduction with H_2. *ACS Catal.* **2021,** *11* (1), 283-289.
37. Liu, C.; Tang, J.; Chen, H. M.; Liu, B.; Yang, P., A Fully Integrated Nanosystem of Semiconductor Nanowires for Direct Solar Water Splitting. *Nano Lett.* **2013,** *13* (6), 2989-2992.
38. Hollmann, F.; Witholt, B.; Schmid, A., $[Cp*Rh(bpy)(H2O)]^{2+}$: a versatile tool for efficient and non-enzymatic regeneration of nicotinamide and flavin coenzymes. *J. Mol. Catal. B Enzym.* **2002,** *19-20*, 167-176.
39. Kuk, S. K.; Jang, J.; Kim, J.; Lee, Y.; Kim, Y. S.; Koo, B.; Lee, Y. W.; Ko, J. W.; Shin, B.; Lee, J.-K.; Park, C. B., CO_2-Reductive, Copper Oxide-Based Photobiocathode for Z-Scheme Semi-Artificial Leaf Structure. *ChemSusChem* **2020,** *13* (11), 2940-2944.
40. Wang, Q.; Liu, J.; Li, Q.; Yang, J., Stability of Photocathodes: A Review on Principles, Design, and Strategies. *ChemSusChem* **2023,** *16* (9), e202202186.
41. Yang, W.; Prabhakar, R. R.; Tan, J.; Tilley, S. D.; Moon, J., Strategies for enhancing the photocurrent, photovoltage, and stability of photoelectrodes for photoelectrochemical water splitting. *Chem. Soc. Rev.* **2019,** *48* (19), 4979-5015.
42. Cestellos-Blanco, S.; Chan, R. R.; Shen, Y.-x.; Kim, J. M.; Tacken, T. A.; Ledbetter, R.; Yu, S.; Seefeldt, L. C.; Yang, P., Photosynthetic biohybrid coculture for tandem and tunable CO_2 and N_2 fixation. *Proc. Natl. Acad. Sci. U.S.A.* **2022,** *119* (26), e2122364119.
43. Su, Y.; Cestellos-Blanco, S.; Kim, J. M.; Shen, Y.-x.; Kong, Q.; Lu, D.; Liu, C.; Zhang, H.; Cao, Y.; Yang, P., Close-Packed Nanowire-Bacteria Hybrids for Efficient Solar-Driven CO_2 Fixation. *Joule* **2020,** *4* (4), 800-811.

Insert Table of Contents artwork